Chapter 5

Neutron induced $(n, 2n)$ reaction cross section for ^{103}Rh, ^{121}Sb and ^{123}Sb isotopes

5.1. Introduction

Neutron induced (n, xn) reaction cross sections are necessary for activation detectors, which are used to probe the energy components of neutron flux. The nuclear data such as cross section, half-life, decay modes, decay radiation properties, γ-ray from radionuclides of the various radioisotopes are widely used in nuclear medicine, radiation shielding, fusion/fission reactor design, radioactive waste disposal and transmutation, radiation safety, *etc.* The neutron induced reaction cross section data of different nuclei is often used to predict the various theoretical nuclear models. The compound nucleus, direct and pre-equilibrium emission are the different models used to understand the reaction mechanism, and the optimum parameters are needed to understand these processes. Therefore, it is essential to improve the accuracy of measured experimental data and understand these reaction models. Recently, several articles on nuclear reactions at moderate excitation energies have been concerned with the emission of particles before the nucleus reaches statistical equilibrium. In theoretical calculations from statistical codes, selecting suitable models is important for obtaining the correct cross sections values [1, 2].

Some of the isotopes of antimony that are made when nuclear fission happens have been found to be the nuclides of the fission product. The cross section data of neutron induced reactions of antimony are very important for the decommissioning of light-water nuclear reactors. Therefore, fast neutron induced cross section measurements with better accuracy for antimony are essential for improving nuclear data. It was observed that when antimony alloy was added to the lead, this increased the hardness and mechanical strength of the lead, and this lead-antimony alloy is used in radiation shielding. The $^{123}\mathrm{Sb}(n, 2n)^{122}\mathrm{Sb}$ reaction produced $^{122}\mathrm{Sb}$ ($\tau_{1/2} = 2.47\ day$) nuclei and the essential radiotracers were used to

study food crops and environmental contamination. Natural antimony is also used in the start-up of the neutron source [3-4]. The neutron induced reactions that result in the formation of various isomers of residual nuclei are crucial for better understanding the role of nuclear structure in the compound nucleus reaction process. In comparison to the ground state of $^{120}Sb^{g}$ and $^{122}Sb^{g}$ with spin $J^{\pi} = 1^{+}$ and $J^{\pi} = 2^{-}$, the $^{120}Sb^{m}$ and $^{122}Sb^{m}$ are high spin isomers with a spin value of $J^{\pi} = 8^{-}$ respectively. Due to the high spin value 8^{-} of the isomeric state relative to the ground state 1^{+} and 2^{-} values, the spin distribution of the residual nucleus can be studied with great sensitivity [5].

Rhodium is an inert transition metal that has a single naturally occurring isotope ^{103}Rh (100%) and is used as an alloying agent to harden palladium and platinum. The ^{103}Rh is used for radiochemical diagnosis of integrated neutron fluence since nuclear reactions (n,γ), $(n,2n)$ and $(n,3n)$ lead to different radioactive isotopes of rhodium with lifetimes in the useful range for activation measurements. Threshold reactions such as (n,n') and $(n,2n)$ have been widely used in foil activation techniques to determine the differential flux (dQ/dE) from neutron sources. An example of such an activation detector is rhodium, which is considered as a monoisotopic [6].

The $(n,2n)$ reaction cross section of the ^{103}Rh, ^{121}Sb and ^{123}Sb isotopes are essential for neutron multiplication calculations. In recent years, the $^{103}Rh(n,2n)^{102}Rh$, $^{121}Sb(n,2n)^{120}Sb$ and $^{123}Sb(n,2n)^{122}Sb$ reaction cross section within 13 to 20 MeV energy range were measured by several authors as mentioned in the EXFOR compilation [7]. The available experimental and evaluated data for the $^{103}Rh(n,2n)^{102}Rh$, $^{121}Sb(n,2n)^{120}Sb$ and $^{123}Sb(n,2n)^{122}Sb$ reactions from threshold to 20 MeV show disagreement at the same incident energy. Since there are significant discrepancies in the measured cross section and evaluated data from different libraries for common incident neutron energy, it is difficult to refine and correct various statistical parameters.

The excitation functions of the $^{121}Sb(n,2n)^{120}Sb^{m}$ and $^{123}Sb(n,2n)^{122}Sb$ reactions were measured at 12.50, 15.79 and 18.87 MeV neutron energies, whereas the $^{103}Rh(n,2n)^{102}Rh^{m}$, $^{103}Rh(n,2n)^{102}Rh^{g}$ and $^{103}Rh(n,2n)^{102}Rh$ reactions cross sections were measured at 16.86 and 19.81 MeV neutron energies relative to the standard $^{27}Al(n,\alpha)^{24}Na$ reference monitor reaction cross section taken from the IRDFF-II database [8]. The experimental results of the present work were compared with the literature data available in the EXFOR database and the latest evaluated data of the JENDL-5.0, FENDL-3.2b, CENDL-3.2, JEFF-3.3, JENDL/AD-2017, ENDF/B-VIII.0 and TENDL-2019 libraries [9-15]. Specifically, the uncertainties in the

measured cross sections data were obtained through the covariance analysis method, which involves uncertainties from each source. In addition, a systematic study of $(n, 2n)$ reaction cross sections for antimony and rhodium isotopes were also done using different formulas given by several authors. The isomeric cross section ratio (σ_m/σ_g) for the $(n, 2n)$ reaction was studied theoretically in the energy range 10–26 MeV from the TALYS (ver. 1.9) [16] and EMPIRE (ver. 3.2.2) [17] codes. The present measurements and available literature data were compared with theoretical predictions performed using the two codes. Furthermore, the different theoretical models from these two codes were used to study the pre-equilibrium process mechanism and the contribution to the current interest reaction channels. The main reason for measuring the $(n, 2n)$ reaction cross section of ^{121}Sb ^{123}Sb and ^{103}Rh isotopes was the lack of sufficient data at higher neutron energies.

5.2. Theoretical calculations using the EMPIRE and TALYS codes for the Antimony (Sb) and Rhodium (Rh)

The theoretical calculations of the $^{121}\mathrm{Sb}(n, 2n)^{120}\mathrm{Sb}^{m}$, $^{121}\mathrm{Sb}(n, 2n)^{120}\mathrm{Sb}^{g}$ and $^{121}\mathrm{Sb}(n, 2n)^{120}\mathrm{Sb}$, $^{123}\mathrm{Sb}(n, 2n)^{122}\mathrm{Sb}^{m}$, $^{123}\mathrm{Sb}(n, 2n)^{122}\mathrm{Sb}^{g}$ and $^{123}\mathrm{Sb}(n, 2n)^{122}\mathrm{Sb}$ reactions as well as the $^{103}\mathrm{Rh}(n, 2n)^{102}\mathrm{Rh}^{m}$, $^{103}\mathrm{Rh}(n, 2n)^{102}\mathrm{Rh}^{g}$ and $^{103}\mathrm{Rh}(n, 2n)^{102}\mathrm{Rh}$ reactions cross section were performed by the statistical nuclear reaction codes TALYS (ver. 1.9) and EMPIRE (ver. 3.2.2) from reaction threshold to 26 MeV energies.

In the above calculations, the different nuclear level densities, pre-equilibrium models and other input parameters are given in both codes and these models and parameters were used to analyze and predict $(n, 2n)$ reaction cross section for ^{103}Rh, ^{121}Sb and ^{123}Sb isotopes. Concerning theoretical calculations with both codes, the different phenomenological and microscopic models used for the estimation of the cross sections are mentioned in Table 5.1. The compound nucleus reaction cross sections were calculated in the framework of the Hauser-Feshbach theory in both codes. The effects of pre-equilibrium emission contribution at higher energies were included in the calculations by considering the classical and quantum mechanical approaches as mentioned in both codes. Similarly, the width fluctuation corrections were considered by considering the Hofmann, Richert, Tepel and Weidenmuller model (HRTW) up to an incident neutron energy of 3 MeV for the correlation between the incident and exit channels in elastic scattering. Furthermore, the γ-ray strength functions were described via Brink-Axel and Kopecky-Uhl generalized Lorentzian with parameters available

in the RIPL-3 database [18] considered for the γ-ray emission, whereas the optical potential models of the Koning and Delaroche were included for the optical potential. The phenomenological and microscopic level density models were used with the optical potential, γ-ray strength function and preequilibrium model to reproduce the measured data and these models are mentioned in Tables 5.2 and 5.3. A more detailed description of these theoretical models is mentioned in Chapter 4.

Table 5.1 The different phenomenological and microscopic models of the optical potential, level densities and γ-ray strength function.

Parameter	Phenomenological models	Semi microscopic models
OMP (n)	(1) (KD): Dispersive, global and local model of Koning and Delaroche	(2) (JLM/Bc): Improved semi microscopic OMP of Bauge, Delaroche, and Girod at low energies
NLD	(1) (CTFG): Constant temperature Fermi gas (2) (BSFG): Back-shifted Fermi gas (3) (GSM): Generalized superfluid model	(4) (HFBCS): Hartree-Fock-BCS (5) (HFB): Hartree-Fock-Bogolyubov (6) (HFB/T): Temperature-dependent Hartree-Fock-Bogolyubov
γ-SFs	(1) (KU): Generalized Lorentzian of Kopecky and Uhl (2) (BA): Generalized Lorentzian of Brink and Axel	(3) (HFBCS/QRPA): Hartree-Fock-BCS–quasiparticle random phase approximation (4) (HFB/QRPA): Hartree-Fock-Bogolyubov–quasiparticle random phase approximation (5) (HG): Hybrid model of Goriely (6) (HFB/T): Temperature-dependent Hartree-Fock-Bogolyubov (7) (RMF/T): Temperature-dependent RMF (8) (D1M/HFB/QRPA): Gogny D1M Hartree-Fock-Bogolyubov–quasiparticle random-phase approximation

Table 5.2 The statistical models and parameterizations of the TALYS (ver. 1.9) code were used to calculate $(n, 2n)$ reaction cross section of ^{103}Rh, ^{121}Sb and ^{123}Sb isotopes.

Optical model	Level density models	Pre-equilibrium model	*E*1 γ-ray strength function model
Koning-Delaroche local potential	Constant temperature model Back-shifted Fermi gas model Generalized superfluid model S. Goriely (microscopic model 1) S. Goriely-S. Hilaire (microscopic model 2) S. Goriely-S. Hilaire Gogny force (microscopic model 3)	Exciton model: (Numerical transition rates with energy-dependent matrix)	Kopecky-Uhl generalized Lorentzian

Table 5.3 The statistical models and parameterizations of the EMPIRE (ver. 3.2.2) code were used to calculate $(n, 2n)$ reaction cross section of ^{103}Rh, ^{121}Sb and ^{123}Sb isotopes.

Optical model	Level density models	Pre-equilibrium models	*E*1 γ-ray strength function model
Koning-Delaroche global potential	EMPIRE-specific level density (ESLM) Constant temperature model (GCM) Generalized superfluid model (GSM) Hartree-Fock Bogoliubov model (HFBM)	Exciton model: PCROSS code, Quantum mechanical models: Multistep compound (MSC), Multistep direct (MSD)	Brink-Axel model

It is found that the relative feeding of the isomeric and ground states can be used as a probe to investigate the spin distribution of the populated excited states of the compound nucleus. The spin cut-off parameter σ_F^2 represents the width of the angular momentum distribution of the level density and is given by the following equation:

$$\sigma_F^2(E_x) = 0.01389(A^{5/4}/\hat{\alpha})\sqrt{\alpha U} \qquad (1)$$

where A is the mass number, U is the effective excitation energy defined as $U = (E_x - \Delta)$, E_x is the true excitation energy and the energy shift Δ is an empirical parameter that is equal to, or for certain models, closely equivalent to, the pairing energy that is used to represent observed odd-even effects in nuclei. The parameter α is the energy dependent level density parameter, which considers shell effects at low energies and the damping at higher excitation energy. When shell effects are absent, the parameter $\hat{\alpha}$ is called the asymptotic level density parameter and is equal to the α parameter. The TALYS keyword "Rspincut" was modified (default Value=1.0) to reproduce the existing experimental data. This keyword represents a multiplication factor of the spin cut-off parameter σ_F^2. Moreover, the basic keywords and the corresponding values used in the input file of the TALYS (ver. 1.9) and EMPIRE (ver. 3.2.2) codes to reproduce the cross sections of neutron induced reactions on ^{103}Rh, ^{121}Sb and ^{123}Sb are given in Tables 5.4 and 5.5.

Table 5.4 Basic keywords and corresponding values used in the input file of the TALYS 1.9 code to reproduce the cross sections of neutron induced reactions on ^{103}Rh, ^{121}Sb and ^{123}Sb.

TALYS 1.9 input for ^{103}Rh ^{121}Sb and ^{123}Sb

Keywords	Value (^{121}Sb)	Value (^{123}Sb)	Value (^{103}Rh)
projectile	n	n	n
element	Sb	Sb	Rh
mass	121	123	103
energy	energies	energies	energies
ldmodel	1	1	1
widthmode	2	2	1
preeqmode	2	2	2
strength	1	1	1
preequilibrium	y	y	y

outpreequilibrium	y	y	y
outbasic	y	y	y
outdensity	y	y	y
filedensity	y	y	y
outgamma	y	y	y
outomp	y	y	y
components	y	y	y
rspincut	0.6	0.6	1.0

Table 5.5 Basic keywords and corresponding values used in the input file of the EMPIRE 3.2.2 code to reproduce the cross sections of neutron induced reactions on ^{103}Rh, ^{121}Sb and ^{123}Sb.

EMPIRE 3.2.2 input for ^{103}Rh, ^{121}Sb and ^{123}Sb

Keywords	Value (^{121}Sb and ^{123}Sb)	Value (^{103}Rh)
LEVDEN	0,1,2,3	0,1,2,3
DIRECT	0	0
HRTW	3	3
GSTRFN	1	1
OMPOT (n)	2405	2405
OMPOT (p)	5405	5405
PCROSS	1.5	1.5
MSC	1	0
MSD	1	0

5.3. Results and discussion of Antimony (Sb) and Rhodium (Rh)

5.3.1 Antimony (Sb)

The experimental data obtained in the present work are discussed and compared with the literature data and results from the available evaluations: TENDL-2019, JEFF-3.3, JENDL/AD-2017, and ENDF/B-VIII.0 databases. The small contribution to the γ-ray activity of products from the ^{121}Sb$(n,\gamma)^{122}$Sb reaction can be ignored due to the very small cross section of the (n,γ) reaction above the 9 MeV energy region. In the present work, further study of the existing experimental cross section data for populating ^{120}Sb and ^{122}Sb ground and the isomeric state as well as the total were also discussed and compared with the theoretical calculations obtained from the TALYS (ver. 1.9) and EMPIRE (ver. 3.2.2) codes.

5.3.1.1 ^{121}Sb$(n,2n)^{120}$Sb^{m}, ^{121}Sb$(n,2n)^{120}$Sb^{g} and ^{121}Sb$(n,2n)^{120}$Sb reactions

There is no evaluation cross section in the database of IAEA for the ^{121}Sb$(n,2n)^{120}$Sb^{m}, ^{121}Sb$(n,2n)^{120}$Sb^{g} reactions. However, the results of the present measurements cross sections at 12.50, 15.79 and 18.87 MeV neutron energies are plotted in Fig. 5.1(a) along with all other reported data. We can see from Fig. 5.1(c) that the trends of these evaluation excitation curves of JEFF-3.3, TENDL-2019, JENDL/AD-2017 and ENDF/B-VIII.0 are not the same.

For the isomeric state cross section from Fig. 5.1(a), our results are higher than those obtained by N. L. Das *et al.* [19], W. D. Lu *et al.* [20] and A. Reggoug *et al.* [31]. At 15.79 and at 18.87 MeV, the present measured data agree with the results of S. K. Ghorai *et al.* [21] and M. Bormann *et al.* [24] within experimental uncertainties. In contrast, at 12.50 MeV, the present data falls between the results of S. K. Ghorai *et al.* [21] and Y. Kanda [30]. Furthermore, for the isomeric state, the cross section values of J. L. Casanova [27] are much higher than the present measured cross section. Similarly, the reported measurements of the various experiments for ^{121}Sb$(n,2n)^{120}$Sb^{g} reaction agree very well except for some of the reported data by R. A. Jarjis [25] and C. Carles [34] as shown in Fig. 5.1(b).

It can be seen from Fig. 5.1(c) that in the 14 to 20 MeV energy range, the results of N. L. Das *et al.* [19], M. Bormann *et al.* [24] and Y. Kanda [30] are consistent with the result of the ENDF/B-VIII.0 evaluation for the ^{121}Sb$(n,2n)^{120}$Sb reaction. In addition, the JENDL/AD-2017 and TENDL-2019 evaluations agree with the reported data of J. H. Mccrary *et al.* [28] and Y. Kanda [30] at higher energies within experimental uncertainties.

The cross section predicted by the JEFF-3.3 library is too large over the 15 MeV energy region and agrees very well with the lower energy data of N. L. Das *et al.* [19], B. Minetti *et al.* [22] and M. Bormann *et al.* [24].

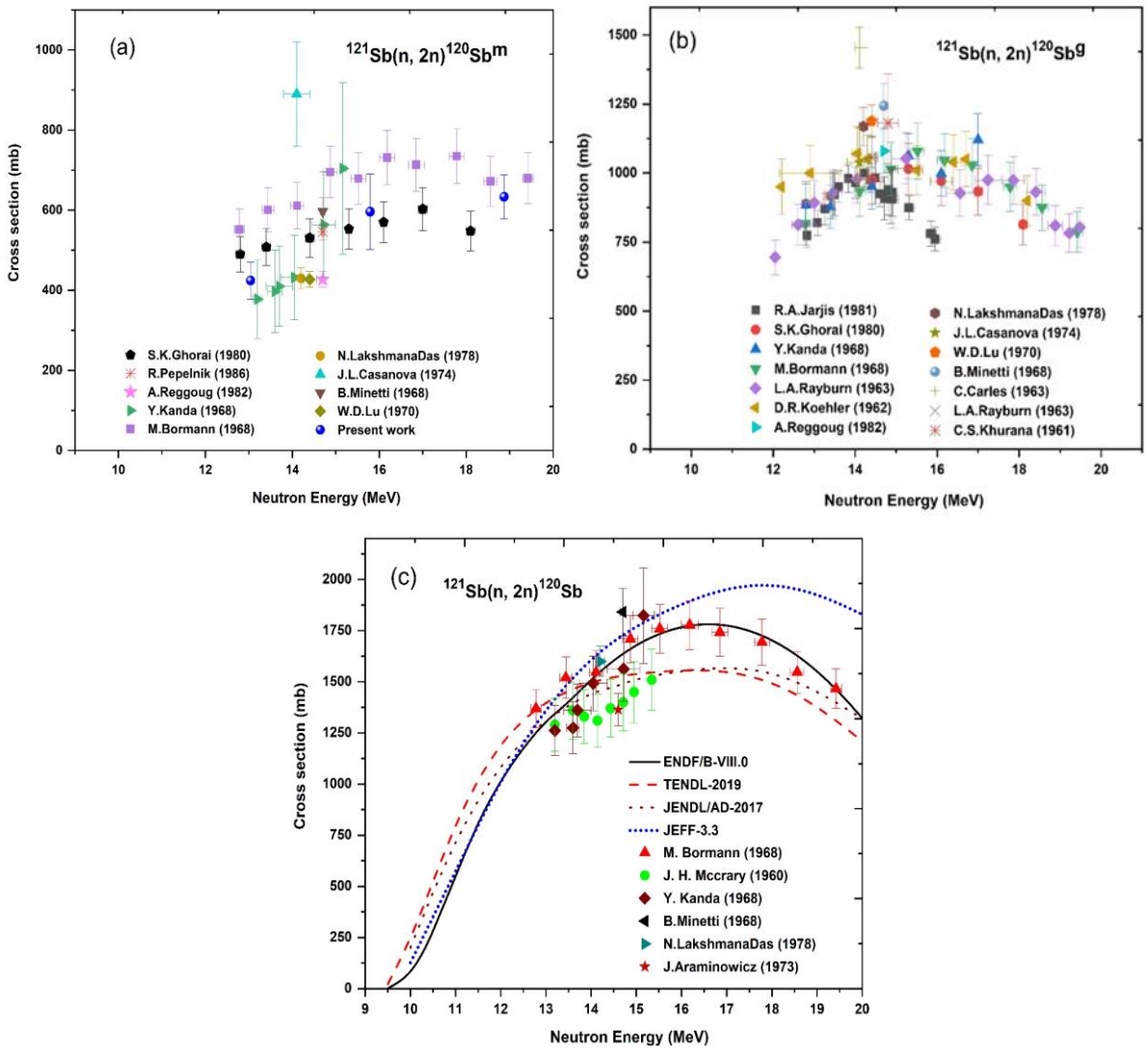

Fig. 5.1 *The comparison of existing literature and evaluated data of the $^{121}Sb(n,2n)^{120}Sb^{m}$, $^{121}Sb(n,2n)^{120}Sb^{g}$ and $^{121}Sb(n,2n)^{120}Sb$ reactions.*

The theoretical calculations from the TALYS and EMPIRE codes utilizing different level density models were performed for the ^{121}Sb$(n,2n)^{120}$Sb^{m}, ^{121}Sb$(n,2n)^{120}$Sb^{g} and ^{121}Sb$(n,2n)^{120}$Sb reactions and results are demonstrated in Fig. 5.2 from threshold to 26 MeV neutron energies. The different statistical models were used in the TALYS and EMPIRE codes for the estimation of cross section and these models are included in Table 5.2 and 5.3.

For the isomeric state, the theoretical TALYS calculations based on three phenomenological level density models agree with the results of N. L. Das *et al.* [19] and W. D. Lu *et al.* [20]. However, our results at 12.50, 15.79 and 18.87 MeV and reported data [21-24] are much higher than those of the three phenomenological models for the $^{121}\mathrm{Sb}(n,2n)^{120}\mathrm{Sb}^{m}$ reaction. The three phenomenological level density models for the $^{121}\mathrm{Sb}(n,2n)^{120}\mathrm{Sb}^{g}$ reaction can reproduce the reported experimental data very well within the experimental uncertainties.

The TALYS calculations using microscopic level density models S. Goriely and S. Goriely-S. Hilaire for the $^{121}\mathrm{Sb}(n,2n)^{120}\mathrm{Sb}^{m}$ reaction can reproduce the experimental data of S. K. Ghorai *et al.* [21], B. Minetti *et al.* [22] and R. Pepelnik *et al.* [23] within experimental uncertainties. In the 13 to 18 MeV energy range, the results of S. K. Ghorai *et al.* [21] and M. Bormann *et al.* [24] are consistent with the results of TALYS calculations using the microscopic level density model S. Goriely-S. Hilaire Gogny for the isomeric state, whereas for the ground state the S. Goriely and S. Goriely-S. Hilaire level density model's calculations agree with the existing experimental data. In addition, for the isomeric state, the TALYS calculation using the microscopic level density model S. Goriely-S. Hilaire Gogny overestimated the cross section and agreed with the lower energies data of S. K. Ghorai *et al.* [21] and M. Bormann *et al.* [24]. In contrast, for the $^{121}\mathrm{Sb}(n,2n)^{120}\mathrm{Sb}^{g}$ reaction, this model underestimated the cross section within 11 to 22 MeV of neutron energies and agreed only with R. A. Jarjis [25] at 16 MeV energies. The TALYS calculations using the microscopic level density model of S. Goriely for the isomeric state and the phenomenological level density model of back-shifted Fermi gas for the ground state shows overall agreement with the present work and existing data as shown in Figs. 5.2(a) and 5.2(b).

Furthermore, our results at 12.50, 15.79 and 18.87 MeV energies agree very well with the EMPIRE calculation using the ESLD level density model as plotted in Fig. 5.2(a). However, the results of EMPIRE calculations using the GSM, GCM and HFBM level density models agree with the reported data within experimental uncertainties for the $^{121}\mathrm{Sb}(n,2n)^{120}\mathrm{Sb}^{m}$ reaction. Similarly, the EMPIRE calculation using the GCM level density model describes the data reasonably well for the ground state, as shown in Fig. 5.2(b). In contrast, the experimental results of the $^{121}\mathrm{Sb}(n,2n)^{120}\mathrm{Sb}^{g}$ reaction agree with the ESLD and HFBM models calculations, whereas the GSM model calculation agrees with the reported data. The measurements of the various experimenters agree very well with each other except

for some of the measurements reported by R. A. Jarjis [25] and C. Carles [34] for the $^{121}\mathrm{Sb}(n,2n)^{120}\mathrm{Sb}^{g}$ reaction.

However, the results of the $^{121}\mathrm{Sb}(n,2n)^{120}\mathrm{Sb}$ reaction, the theoretical calculations from the TALYS code based on the generalized superfluid and back-shifted Fermi gas models describe the data of J. H. Mccrary *et al.* [28], J. Araminowicz *et al.* [29] and Y. Kanda [30] within 13 to 14 MeV energy range. In contrast, the constant temperature model can describe Y. Kanda [30] within the 14 to 15 MeV energy range, data of J. H. Mccrary *et al.* [28] at 15.34 MeV and lower data of M. Bormann *et al.* [24]. In addition, the TALYS calculations based on the microscopic models agree very well with J. H. Mccrary *et al.* [28], J. Araminowicz *et al.* [29] and Y. Kanda [30] within the 13 to 14 MeV energy range. The TALYS calculation using S. Goriely-S. Hilaire Gogny's microscopic models is plotted in Fig. 5.2(c).

Furthermore, the EMPIRE calculation using the GSM can describe the data of N. L. Das *et al.* [19], M. Bormann *et al.* [24] for the $^{121}\mathrm{Sb}(n,2n)^{120}\mathrm{Sb}$ reaction. In contrast, the EMPIRE calculations using the GCM and microscopic HFBM models can describe the data of Y. Kanda [30] at 14.05 and 14.72 MeV and data of M. Bormann *et al.* [24] from 12.78 to 19.42 MeV energies within experimental uncertainties. The EMPIRE calculation using the GCM level density model describes the reported data as shown in Fig. 5.2(c).

The contributions of the cross sections from different reaction processes in the $^{121}\mathrm{Sb}(n,2n)^{120}\mathrm{Sb}$ reaction were studied from threshold to 30 MeV neutron energies. It is observed that the contribution of the pre-equilibrium process increases with energy above 19 MeV. The contribution from the direct process is zero in the reaction cross section and the compound nucleus process contributes the maximum cross section. The more significant pre-equilibrium emission leads to a reduction in the compound nucleus emission. To investigate the effect of the pre-equilibrium emission at higher energy, the theoretical calculations were performed by the EMPIRE code. Therefore, a more detailed comparison of the EMPIRE calculations using different pre-equilibrium and level density models for the $^{121}\mathrm{Sb}(n,2n)^{120}\mathrm{Sb}$ reaction is illustrated in Fig. 5.2(c). In the present work, the two quantum-mechanical pre-equilibrium models (i) Multi-Step Compound (MSC), (ii) Multi-Step Direct (MSD) were used to study the pre-equilibrium emission from EMPIRE code along with generalized superfluid, Gilbert Cameron and Hartree-Fock level density models. However, the results of the $^{121}\mathrm{Sb}(n,2n)^{120}\mathrm{Sb}$ reaction, the MSC pre-equilibrium model with a generalized superfluid, Gilbert Cameron and Hartee-Fock level density models are describing

the data of M. Bormann *et al.* [24] up to 16 MeV. In contrast, the MSD pre-equilibrium model with a generalized superfluid, Gilbert Cameron and Hartee-Fock level density models agree very well with the lower energy data of N. L. Das *et al.* [19], M. Bormann *et al.* [24] and Y. Kanda [30]. The best theoretical excitation curve for $^{121}\mathrm{Sb}(n,2n)^{120}\mathrm{Sb}$ reaction with the MSD pre-equilibrium and Gilbert Cameron level density model is plotted in Fig. 5.2(c).

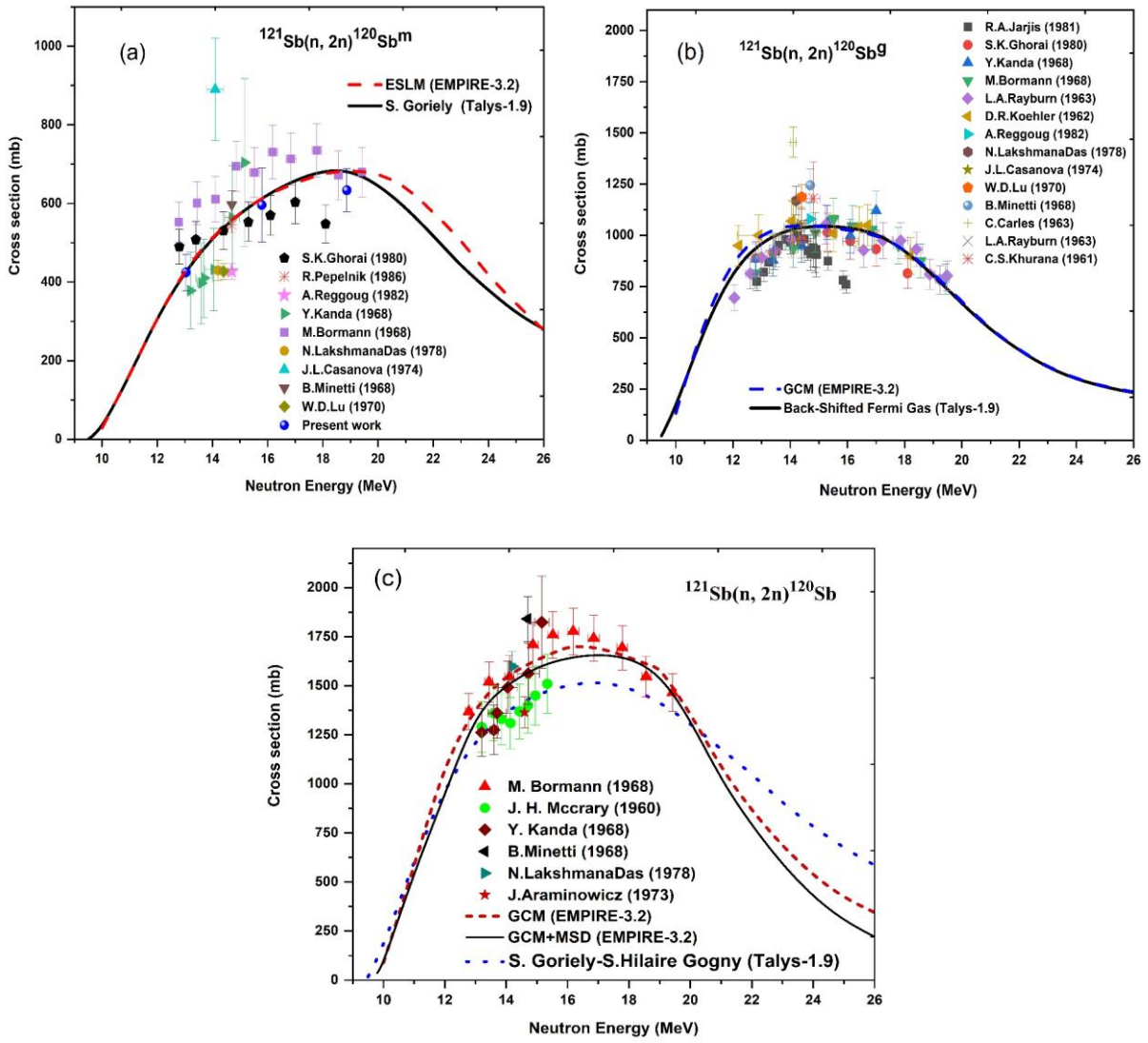

Fig. 5.2 *The experimental data of the $^{121}Sb(n,2n)^{120}Sb^{m}$, $^{121}Sb(n,2n)^{120}Sb^{g}$ and $^{121}Sb(n,2n)^{120}Sb$ reactions and theoretical calculations from the TALYS and EMPIRE codes using different level density models.*

5.3.1.2 $^{123}\mathrm{Sb}(n,2n)^{122}\mathrm{Sb}^{m}$, $^{123}\mathrm{Sb}(n,2n)^{122}\mathrm{Sb}^{g}$ and $^{123}\mathrm{Sb}(n,2n)^{122}\mathrm{Sb}$ reactions

It is observed that for the $^{123}Sb(n,2n)^{122}Sb^{m}$ and $^{123}Sb(n,2n)^{122}Sb^{g}$ reactions experimental data are exist within the 13-16 MeV neutron energies. The reported experimental results of J. L. Casanova [27], E. Rurarz *et al.* [37] and S. K. Mangal *et al.* [38] are slightly higher than the N. L. Das *et al.* [19] and J. Luo *et al.* [26] for the isomeric state. However, the data of J. Luo *et al.* [26] agrees with the N. L. Das *et al.* [19] as shown in Fig. 5.3(a). Similarly, we can see from Fig. 5.3(b) that for the ground state, the results of B. Minetti *et al.* [22] and C. S. Khurana *et al.* [35] are slightly higher than the J. Luo *et al.* [26] and J. L. Casanova [27]. However, the results of J. Luo *et al.* [26] is consistent with the J. L. Casanova [27] within experimental error.

From Fig. 5.3(c), we can see that in the 13 to 19 MeV energy range our data at 12.50, 15.79 and 18.87 MeV are consistent with the result of the JENDL/AD-2017 evaluated data for the $^{123}Sb(n,2n)^{122}Sb$ reaction. At 15.79 and 18.87 MeV, the present measured data agree with the results of the TENDL-2019 evaluated data, whereas at 12.50 MeV the present measurements data agree with the ENDF/B-VIII.0 evaluated data, as we can see from Fig. 5.3(c). However, the results of W. D. Lu *et al.* [20] and S. K. Ghorai *et al.* [21] agree with the result of the JENDL/AD-2017 evaluation within the experimental uncertainties. Similarly, the results of N. L. Das *et al.* [19] and J. Luo *et al.* [26] are agrees very well with the JEFF-3.3 evaluation.

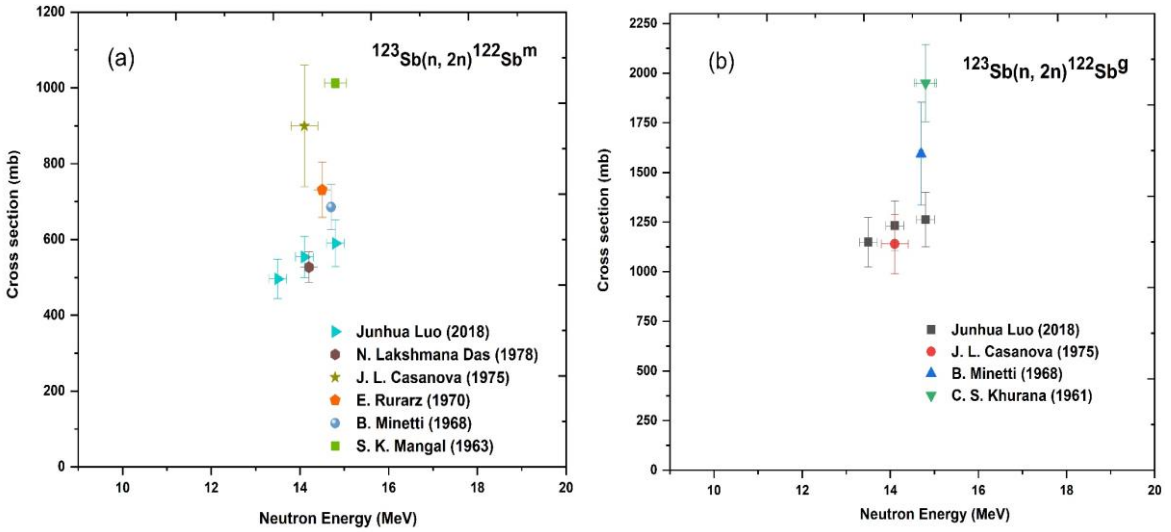

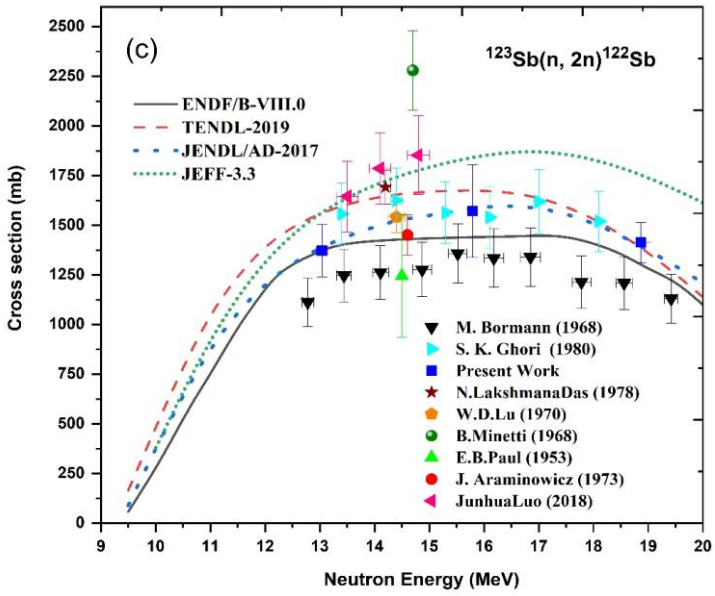

Fig. 5.3 *The comparison of existing literature and evaluated data of the* $^{123}Sb(n,2n)^{122}Sb^{m}$, $^{123}Sb(n,2n)^{122}Sb^{g}$ *and* $^{123}Sb(n,2n)^{122}Sb$ *reactions.*

The existing experimental data of the ^{123}Sb$(n,2n)^{122}$Sb^{m}, ^{123}Sb$(n,2n)^{122}$Sb^{g} and ^{123}Sb$(n,2n)^{122}$Sb reactions and the theoretical calculations from the TALYS and EMPIRE codes using different level density models are illustrated in Fig. 5.4 from threshold to 26 MeV neutron energies. The different statistical models used in the calculations are included in Tables 5.2 and 5.3.

It is observed that cross section for the isomeric state, the theoretical calculations from TALYS based on the three phenomenological level density models failed to reproduce the experimental data. In contrast, the TALYS calculations using three microscopic level density models agree very well with the experimental data reported by N. L. Das *et al.* [19] and J. Luo *et al.* [26] and microscopic calculation based on the S. Goriely-S. Hilaire Gogny model is plotted in Fig. 5.4(a).

However, the cross section of the ^{123}Sb$(n,2n)^{122}$Sb^{g} reaction, the TALYS calculation based on the constant temperature level density model is less satisfied with the literature data of J. Luo *et al.* [26] and agrees very well with the J. L. Casanova [27] for default Rspincut=1.0 parameter, by reducing the values of Rspincut=0.6, this model is in agreement with higher energies data of J. Luo *et al.* [26] as shown in Fig. 5.4(b). However, the results of TALYS calculations using the back-shifted Fermi gas and generalized superfluid level density models are lower than the experimental results. In addition, the TALYS calculations

using three microscopic level density models are fails to describe the experimental data for the ground state.

The EMPIRE calculation using the ESLM level density model describes the $^{123}Sb(n,2n)^{122}Sb^{g}$ reaction cross section reasonably well as shown in Fig. 5.4(b). In contrast, the theoretical values from the EMPIRE using the GCM, GSM and HFBM level density models are much higher than experimental values. The reported cross section values of the $^{123}Sb(n,2n)^{122}Sb^{m}$ reaction are much higher than those of the theoretical excitation curves from the EMPIRE code using the GCM, GSM and HFBM level density models. The results of the EMPIRE calculation using the HFBM model are plotted in Fig. 5.4(a).

The measured cross sections for the $^{123}Sb(n,2n)^{122}Sb$ reaction at 12.50, 15.79 and 18.87 MeV neutron energies and the results of the TALYS and EMPIRE calculations using different level density models are plotted in Fig. 5.4(c) and measured values are given in Table 3.5 [Chapter 3]. The theoretical calculations from the TALYS code based on the phenomenological level density models describe the data of W. D. Lu *et al.* [20], S. K. Ghorai *et al.* [21] within 15 to 16 MeV energy range. In contrast, the TALYS calculations based on the microscopic level density models S. Goriely and S. Goriely-S. Hilaire agree very well with W. D. Lu *et al.* [20], S. K. Ghorai *et al.* [21], whereas the calculations based on microscopic level density model S. Goriely-S. Hilaire Gogny agrees with the lower energies data of M. Bormann *et al.* [24], J. Arminowicz *et al.* [29] and with higher energies data of S. K. Ghorai *et al.* [21]. Further, the EMPIRE calculation using the GSM model is shown in Fig. 5.4(c) and it is observed that the generalized superfluid model agrees with J. Luo *et al.* [26]. In contrast, the EMPIRE results of Gilbert Cameron and Hartee-Fock level density models are consistent with the N. L. Das *et al.* [19] and lower energies data of the S. K. Ghorai *et al.* [21].

The contribution of the cross sections from different reaction processes in the $^{123}Sb(n,2n)^{122}Sb$ reaction was studied from threshold to 26 MeV neutron energies. It is observed that the contribution of the pre-equilibrium process increases with energy above 19 MeV. The contribution from the direct process is zero in the reaction cross section and the compound nucleus process contributes maximum cross section. The more significant pre-equilibrium emission leads to a reduction in the CN emission. To investigate the effect of the pre-equilibrium emission at higher energy, theoretical calculations were performed with the EMPIRE code. Therefore, a more detailed comparison of the EMPIRE calculations using different pre-equilibrium and level density models for the $^{123}Sb(n,2n)^{122}Sb$ reaction is

illustrated in Fig. 5.4(c). In the present work, two Quantum-mechanical pre-equilibrium models (i) Multi-Step Compound (MSC) (ii) Multi-Step Direct (MSD) were used to study the pre-equilibrium emission from the EMPIRE code along with generalized superfluid, Gilbert Cameron and Hartree-Fock level density models. However, the results of the $^{123}\mathrm{Sb}(n,2n)^{122}\mathrm{Sb}$ reaction, the MSC pre-equilibrium model with a generalized superfluid, Gilbert Cameron and Hartee-Fock level density models can describe the data of J. Luo *et al.* [26]. In contrast, the MSD pre-equilibrium model with a generalized superfluid, Gilbert Cameron and Hartee-Fock level density models agree very well with the data of N. L. Das *et al.* [19], W. D. Lu *et al.* [20] and S. K. Ghorai *et al.* [21] within experimental uncertainties as shown in Fig. 5.4(c).

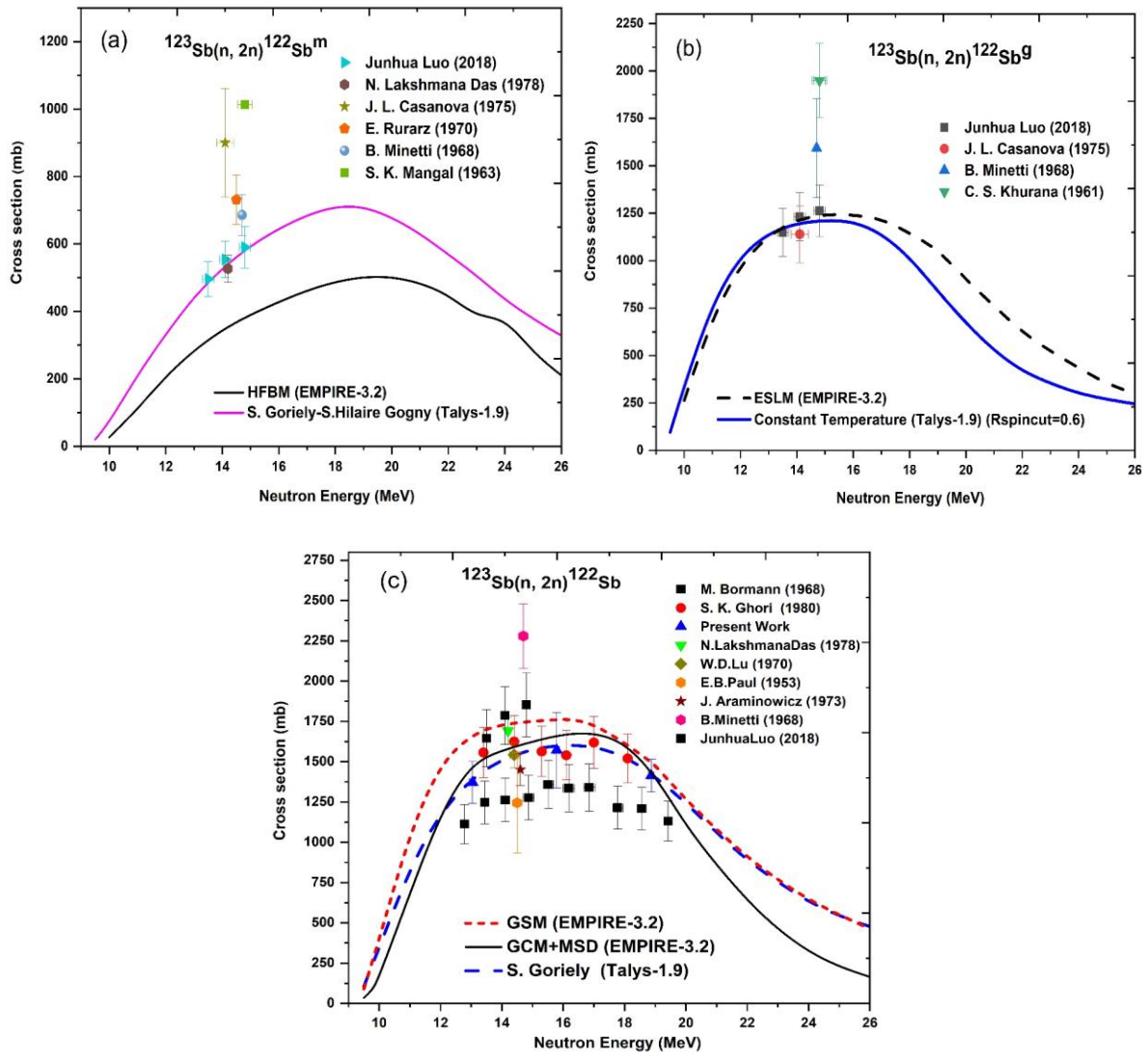

Fig. 5.4 *The experimental data of the $^{123}Sb(n,2n)^{122}Sb^{m}$, $^{123}Sb(n,2n)^{122}Sb^{g}$ and $^{123}Sb(n,2n)^{122}Sb$ reactions and theoretical calculations from the TALYS and EMPIRE codes using different level density models.*

5.3.1.3 Isomeric cross section ratio

The isomeric pairs $^{120}Sb^{m, g}$ and $^{122}Sb^{m, g}$ are formed in the $(n, 2n)$ reaction on ^{121}Sb and ^{123}Sb isotopes. The EMPIRE and TALYS codes were used to calculate the isomeric to ground state cross section ratio (σ_m/σ_g) theoretically. This ratio is low at low energies and increases as the incident particle energy increases, resulting in an increase in the population of high spin levels of the compound nucleus. The reported experimental data and theoretical results of the TALYS and EMPIRE calculations based on the different level density models are shown together in Figs. 5.9(a) and 5.9(b).

For the isomeric pair $^{120}Sb^{m, g}$ the TALYS calculations using three phenomenological level density models agree with the experimental data of W. D. Lu *et al.* [20], Y. Kanda [30] and A. Reggoug *et al.* [31] at lower energy region, whereas at higher energy region the calculated isomeric cross section ratio is retaining the trend of underestimating. In contrast, the TALYS calculations based on the microscopic level density models of S. Goriely and S. Goriely-S. Hilaire reproduce the higher energy data of M. Bormann *et al.* [24], lower energy data of S. K. Ghorai *et al.* [21] and Y. Kanda [30] within experimental uncertainties, whereas the microscopic level density models of S. Goriely-S. Hilaire Gogny overestimated the isomeric cross section ratio in higher energy regions and agreed with only lower energy data of M. Bormann *et al.* [24] and J. L. Casanova [27].

However, the theoretical isomeric cross section ratio from the EMPIRE code based on the GSM, GCM and HFBM level density models agree with the S. K. Ghorai *et al.* [21], Y. Kanda [30] and higher energy data of M. Bormann *et al.* [24] within experimental uncertainties. The results show that the TALYS and EMPIRE calculations using GCM and S. Goriely level density models are described quite well the behaviour of isomeric cross section ratio as shown in Fig. 5.5(a).

For the $^{123}Sb(n, 2n)^{122}Sb^{m}/^{123}Sb(n, 2n)^{122}Sb^{g}$ isomeric cross section ratio literature data exist only in the 13-15 MeV energy region. The theoretical calculations from the TALYS code based on the three phenomenological level density models agree with the data of B. Minetti *et al.* [22] and J. Luo *et al.* [26]. The results show that the back-shifted Fermi gas model describes the isomeric cross section ratio quite well, as shown in Fig. 5.5(b). However, the TALYS calculations based on the three microscopic level density models do not reproduce the reported experimental data.

The theoretical excitation curve from the EMPIRE calculation using the HFBM level density model is lower than the data of B. Minetti *et al.* [22], J. Luo *et al.* [26] and J. L. Casanova *et al.* [27] as shown in Fig. 5.5(b). However, the results of the GCM and GSM level density models does not reproduce the experimental data of the previous work.

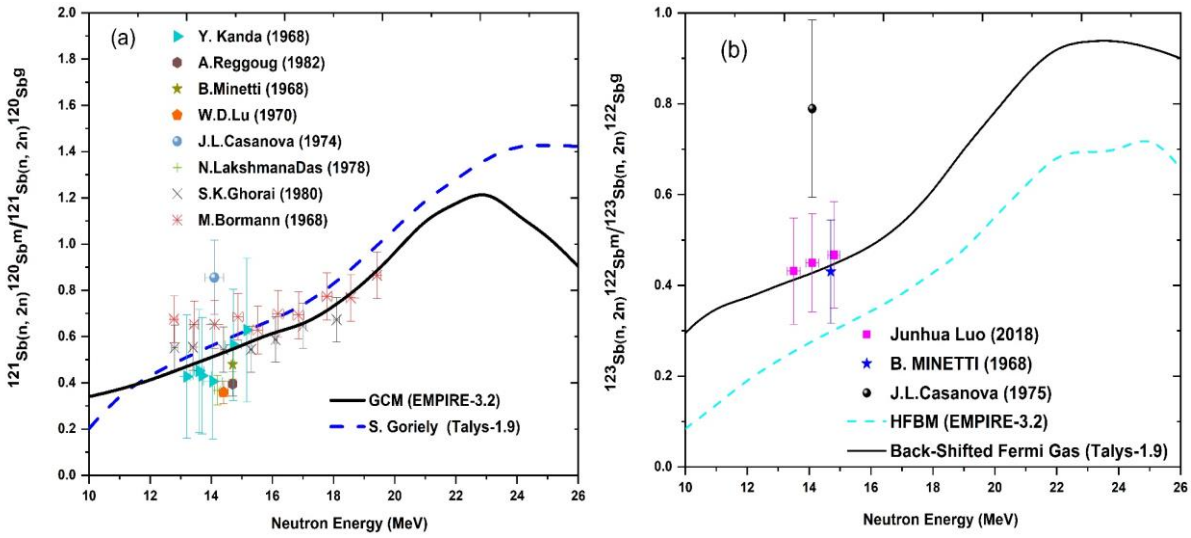

Fig. 5.5 *Isomeric cross section ratio* (σ_m/σ_g) *and theoretical calculations from the TALYS and EMPIRE codes using different level density models.*

5.3.2 Rhodium (Rh)

The ^{103}Rh$(n,2n)^{102}$Rh^{m}, ^{103}Rh$(n,2n)^{102}$Rh^{g} and ^{103}Rh$(n,2n)^{102}$Rh reaction cross section were measured at two different neutron energies. The experimental results of the ^{103}Rh$(n,2n)^{102}$Rh^{m}, ^{103}Rh$(n,2n)^{102}$Rh^{g} reactions and for the total ^{103}Rh$(n,2n)^{102}$Rh reaction which is the sum of both are presented in Table 3.6 [Chapter 3]. The cross sections were compared and discussed with previous literature data taken from the EXFOR compilation and evaluation of the FENDL-3.2b, TENDL-2019, JENDL-5.0 and ENDF/B-VIII.0 libraries. Statistical reaction codes TALYS (ver. 1.95) and EMPIRE (ver. 3.2.3) were used for the theoretical estimations of the reaction cross sections. It is observed that most of the previous measurements were made with β-ray or γ-ray counting using NaI(T1) detector. The γ-ray counting with NaI(T1) detector suffers from a defect of poor resolution. There are very few measurements reported with Ge(Li) detector. Therefore, discrepancies were observed in reported $(n,2n)$ reaction cross sections. The contribution of the pre-equilibrium process at higher energies was done by using different pre-equilibrium models.

5.3.2.3 $^{103}Rh(n,2n)^{102}Rh^{m}$, $^{103}Rh(n,2n)^{102}Rh^{g}$ and $^{103}Rh(n,2n)^{102}Rh$ reactions

The mapping of excitation functions for the $^{103}Rh(n,2n)^{102}Rh^{m}$ and $^{103}Rh(n,2n)^{102}Rh^{g}$ reactions was performed experimentally and theoretically for the first time from the reaction threshold to 25 MeV. These previous measurements reported in the literature [39-44] and present experimental results were used to validate the theoretical estimations of the TALYS (ver. 1.95) code by considering the various level density, preequilibrium, and optical potential models available in the code. The results for the isomeric and ground state cross section based on the phenomenological and microscopic level density models are presented in Figs. 10(a-b) and 11(a-b).

As can be seen, the previous measurements of the isomeric state cross section are only limited to a narrow energy range of 13.5–15.0 MeV [40, 42, 43], whereas the data of N. Fotiades *et al.* [39], A. Paulsen *et al.* [41] and W. D. Lu *et al.* [43] demonstrate significant discrepancies. The theoretical results for the isomeric state cross section based on the phenomenological and microscopic level density models are presented in Fig. 5.6(a-b). The results show that the back-shifted Fermi gas model describes quite well the cross section data of A. A. Filatenkov [40] and J. Laurec *et al.* [42] and it also follows the trend of the present experimental results at 19.89 MeV within experimental uncertainties. However, the generalized superfluid model does not reproduce the experimental data of the present work as well as the previous literature data within 13-18 MeV, whereas the constant temperature model follows the trend of the present experimental results at 16.86 MeV and higher energies data of J. Laurec *et al.* [42]. The microscopic calculations by S. Goriely and S. Goriely-S. Hilaire overestimated the cross section compared to the reported data of A. A. Filatenkov [40] and J. Laurec *et al.* [42] and S. Goriely-S. Hilaire performs very well for the experimental data of the present work at 16.86 MeV. The theoretical trend of the S. Goriely-S. Hilaire Gogny model is less satisfactory compared to the other two microscopic models with the experimental data.

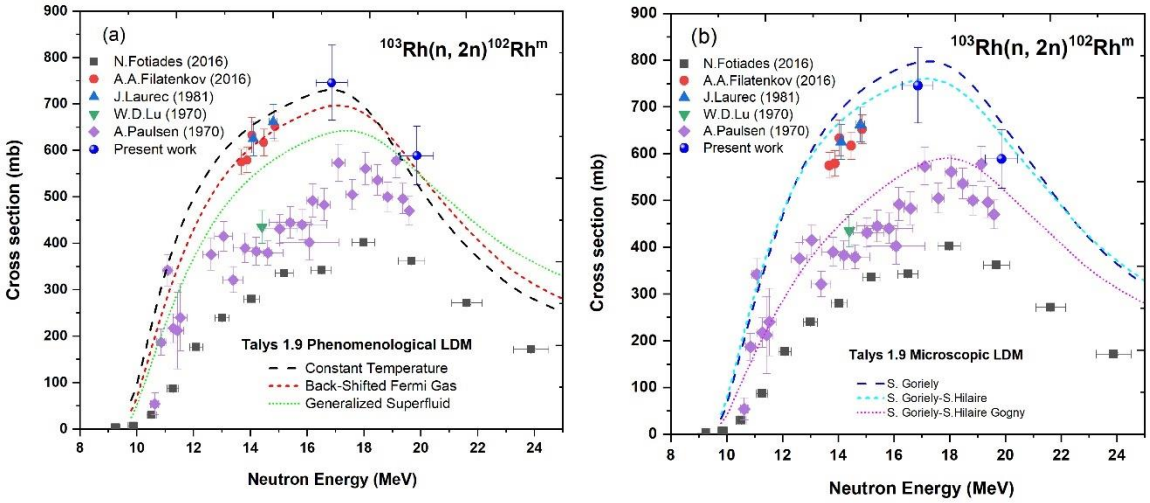

Fig. 5.6 . *Present measurements and reported literature isomeric state cross sections are compared with the TALYS (ver. 1.95) calculations based on the level density models.*

As can be seen, the previous measurements of the ground state cross section also demonstrated significant discrepancies. As shown in Fig. 5.7(a), the ground state results of the back-shifted Fermi gas and generalized superfluid models perform excellently for the present data at 19.89 MeV and the latest data reported by A. A. Filatenkov [40] and M. Bormann *et al.* [44]. The theoretical predictions based on the constant temperature models agree with the data of [39, 42] from the 13-14 MeV region and present experimental results at 16.86 MeV. These theoretical calculations are consistent with most of the literature data and the present experimental work. Similarly, the microscopic calculations for the ground state based on the S. Goriely-S. Hilaire and S. Goriely-S. Hilaire Gogny show good agreement with the reported data of N. Fotiades *et al.* [39], A. A. Filatenkov [40], and M. Bormann *et al.* [44] and present study at 19.89 MeV as shown in Fig. 5.7(b). However, the microscopic calculations for the ground state based on S. Goriely show good agreement with the reported data of the present study at 16.86 MeV.

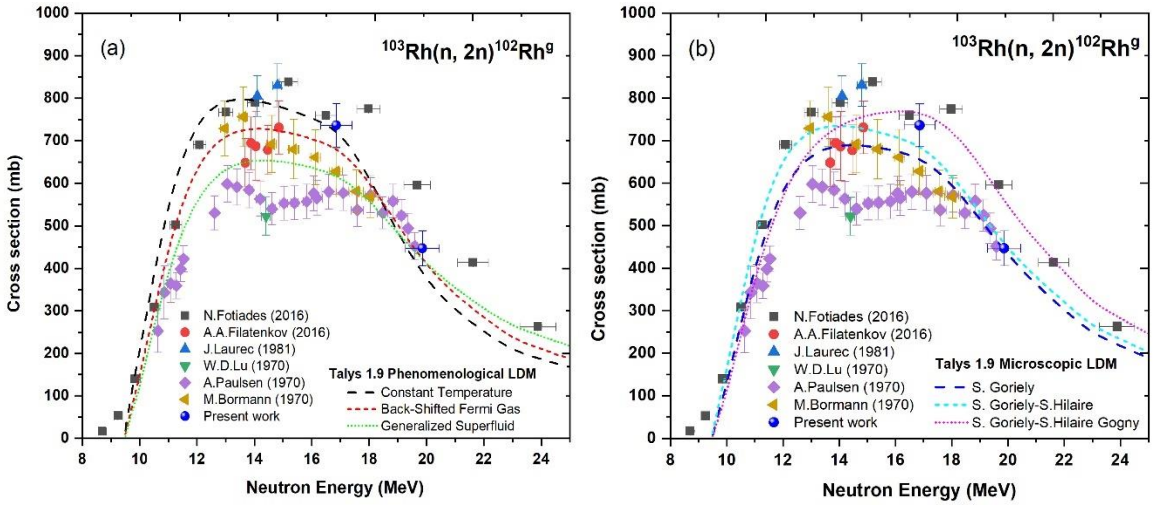

Fig. 5.7 *Present measurements and reported literature ground state cross sections are compared with the TALYS (ver. 1.95) calculations based on the level density models.*

The present experimental results of the ^{103}Rh$(n, 2n)^{102}$Rh reaction are shown in Fig. 5.8 and values are presented in Table 3.6 [Chapter 3] along with their uncertainties. The measured cross sections are compared with literature data [40, 41, 45-49], evaluated data libraries [11, 12, 14, 15] and the theoretical calculations. As can be seen, the measured experimental data of A. A. Filatenkov [40], J. Frehaut *et al.* [45] and L. R. Vesser *et al.* [46] show good agreement with the evaluated data of the ENDF/B-VIII.0 and JENDL-5.0 libraries within experimental uncertainties. Our results at the average neutron energy of 16.86 MeV are higher than the evaluated by the TENDL-2019 data library and show good agreement with the evaluated data of the JENDL-5.0, ENDF/B-VIII.0 and FENDL-3.2b libraries. A good agreement is found between the experimental data of the present work and those of L. R. Vesser *et al.* [46] at 16.86 MeV, whereas the present results at 19.89 MeV follow the trend of the TENDL-2019 and FENDL-3.2b data libraries within experimental uncertainties. In contrast, the reported measured data of A. Paulsen *et al.* [41], D. G. Vallis *et al.* [48] and H. A. Tewes *et al.* [49] show lower values of cross section compared to the latest evaluated data.

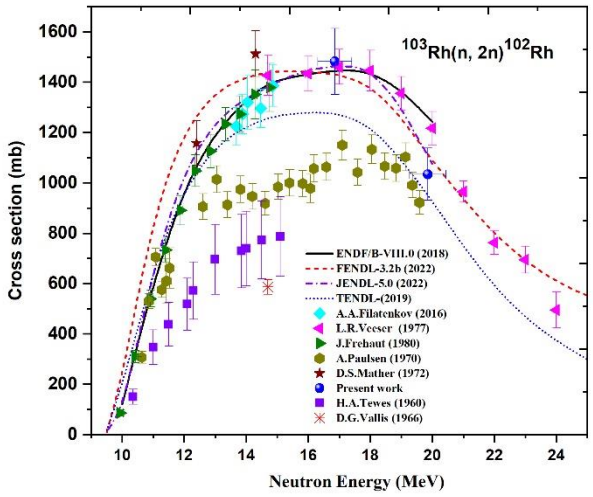

Fig. 5.8 *The present measurements and reported literature cross sections are compared with the latest evaluated data libraries.*

The theoretical results based on the phenomenological and microscopic level density models are shown in Fig. 5.9(a-d). In the case of level density models, almost all recent experimental data are within the range of theoretical calculations, except the data reported by A. Paulsen *et al.* [41], D. G. Villis *et al.* [48] and H. A. Tewes *et al.* [49] above 10 MeV energies. As shown in Fig. 5.9(a), the present measurements at 16.86 and 19.89 MeV are in good agreement with the theoretical calculation based on the constant temperature level density model. The generalized superfluid model fails to reproduce the cross section of A. A. Filatenkov [40], and L. R. Veeser *et al.* [46]. At the near threshold of 13 MeV energies, the theoretical prediction based on the constant temperature model diverges from the experimental data. The back-shifted Fermi gas model calculation is in good agreement with the data of A. A. Filatenkov [40] and the present measurement at 19.89 MeV [see Fig 5.9(a)]. Similarly, the theoretical results of S. Goriely and S. Goriely-S. Hilaire calculations agreed with our results at 16.86 MeV and data of A. A. Filatenkov [40], L. R. Veeser *et al.* [46] and D. S. Mather *et al.* [47], whereas all three microscopic level density models are following the trend of the experimental data of L. R. Veeser *et al.* [46] above 18 MeV [see Fig. 5.9(b)]. Furthermore, the EMPIRE code was also used for theoretical calculations using several models of level density, optical model, and γ-ray strength functions, and the optimal combination of the parameters is given in Table 5.5. Note that among the three phenomenological level density models, the EMPIRE calculations based on the Empire-specific level density model show good agreement with the reported data of A. A. Filatenkov [40], J. Frehaut *et al.* [45] and L. R. Veeser *et al.* [46] as well as present measurements at 16.86 MeV [see Fig. 5.9(c)]. Similarly, the obtained theoretical trends based on the RIPL-3

HFB level density show agreement with the literature data of L. R. Veeser *et al.* [46], D. S. Mather *et al.* [47] and present work at 16.86 MeV [see Fig. 5.9(d)].

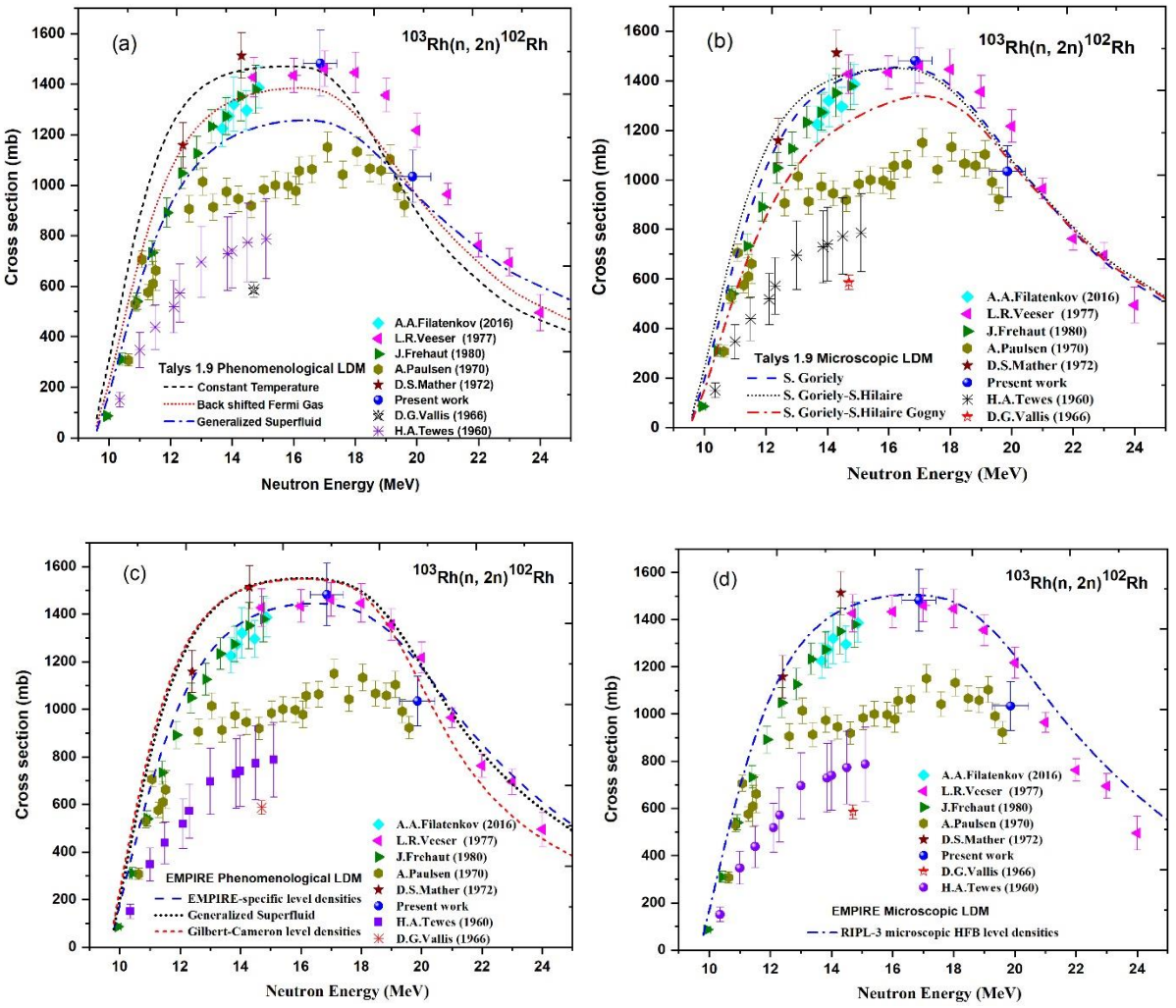

Fig. 5.9 *Present measurements and reported literature cross sections are compared with the TALYS (ver. 1.95) (a and b) and EMPIRE (ver. 3.2.3) (c and d) calculations based on the level density models.*

5.3.2.2 Isomeric cross section ratio

The experimental isomeric cross section ratios obtained in the present work as mentioned in Table 3.6 [Chapter 3] and reported in the literature [40-43], and the results of the theoretical investigation of isomeric cross section ratio (σ_m/σ_g) for the $^{103}\mathrm{Rh}(n,2n)^{102}\mathrm{Rh}^{m}$ and $^{103}\mathrm{Rh}(n,2n)^{102}\mathrm{Rh}^{g}$ reactions based on the phenomenological and microscopic level density models are shown in Fig. 5.10(a-b). This ratio is low in the low energy region and grows as the incident particle energy increases, resulting in a rise in the population of high spin levels of the compound nucleus. The increasing value of the isomeric

cross section ratio with increasing neutron energy is attributed to the higher spin of the isomeric state (6^+) as compared to that of the ground state (1^-, 2^-). As can be seen, all three phenomenological level density models lead to a good agreement of the cross section ratio for the reported of A. A. Filatenkov [40], W. D. Lu *et al.* [43] and lower energies data of A. Paulsen *et al.* [41] within experimental uncertainties as well as good agreement is also found between the experimental data of present work as shown in Fig. 5.10(a), whereas microscopic level density model S. Goriely-S. Hilaire shows agreement only with the data of A. A. Filatenkov [40] as shown in Fig. 5.10(b). The theoretical results of the S. Goriely and S. Goriely-S. Hilaire Gogny models fail to reproduce the experimental data.

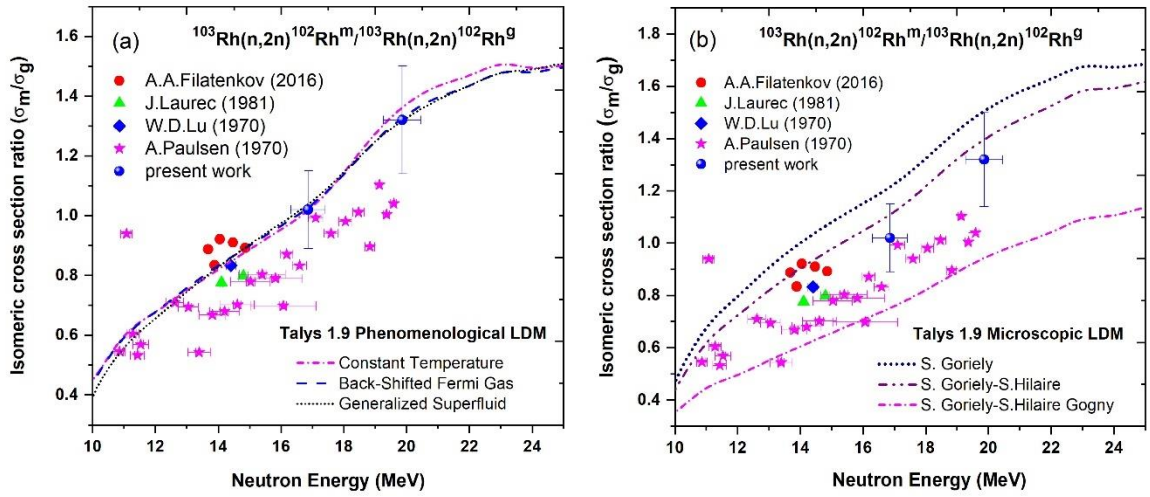

Fig. 5.10 *Measured isomeric cross section ratio (σ_m/σ_g) and TALYS (ver. 1.95) theoretical calculations based on the phenomenological and microscopic level density models.*

5.4. Cross section semi-empirical formulae and results of systematic formulae

The semi-empirical formulae for the $(n, 2n)$ reaction cross section developed by the authors Chatterjee, Lu and Fink, Luo, Bychkov and Habbani [50-54] within 14 to 15 MeV energies. The cross sections of the ^{103}Rh$(n, 2n)^{102}$Rh, ^{121}Sb$(n, 2n)^{120}$Sb and ^{123}Sb$(n, 2n)^{122}$Sb reactions were calculated using the systematic formulae and obtained values are given in Table 5.6 It is observed that $(n, 2n)$ reaction cross sections obtained from formulae of Chatterjee *et al.* [50] and Bychkov *et al.* [53] agree with the literature data of J. H. Mccrary *et al.* [28] and J. Araminowicz *et al.* [29] for the ^{121}Sb$(n, 2n)^{120}$Sb reaction, data of J. Araminowicz *et al.* [29] for the ^{123}Sb$(n, 2n)^{122}$Sb reaction, whereas the cross sections

obtained from formulae of Chatterjee *et al.* [50] agree with the literature data A. A. Filatenkov [40] for the ^{103}Rh$(n,2n)^{102}$Rh reaction. Similarly, the cross sections obtained from the formulae of Luo *et al.* [52] and Lu and Fink [51] agree with the literature data of Y. Kanda [30] for the ^{121}Sb$(n,2n)^{120}$Sb reaction and data of W. D. Lu *et al.* [20] and S. K. Ghorai *et al.* [21] for the ^{123}Sb$(n,2n)^{122}$Sb reaction, whereas for the ^{103}Rh$(n,2n)^{102}$Rh data of A. A. Filatenkov [40] and J. Frehaut *et al.* [45]. In contrast, the $(n,2n)$ reaction cross section obtained from the Habbani *et al.* [54] formulae are much lower compared to other formulae and does not agree with the available literature data for the ^{103}Rh, ^{121}Sb and ^{123}Sb isotopes.

Table 5.6 The $(n,2n)$ reaction cross section for ^{103}Rh, ^{121}Sb and ^{123}Sb isotopes estimated using the systematic formulae.

Authors	^{121}Sb$(n,2n)^{120}$Sb	^{123}Sb$(n,2n)^{122}$Sb	^{103}Rh$(n,2n)^{102}$Rh
Chatterjee	1410	1458	1259
Lu and Fink	1519	1569	1343
Luo	1568	1626	1315
Bychkov	1369	1440	1196
Habbani	1360	1442	1184
JENDL/AD-2017	1471	1533	1405
ENDF/B-VIII.0	1607	1430	1377
TENDL-2019	1524	1659	1249
JEFF-3.3	1621	1709	1434
EXFOR	1364	1853	1296

5.5. Summary and Conclusions

The cross sections for the ^{121}Sb$(n,2n)^{120}$Sb^{m}, ^{123}Sb$(n,2n)^{122}$Sb, ^{103}Rh$(n,2n)^{102}$Rh^{m} ^{103}Rh$(n,2n)^{102}$Rh^{g} and ^{103}Rh$(n,2n)^{102}$Rh reactions were measured using the neutron activation and offline γ-ray spectrometric techniques in the 13-22 MeV energy region relative to the ^{27}Al$(n,\alpha)^{24}$Na reference reaction. The present measured data and statistical cross section from the TALYS (ver. 1.9) and EMPIRE (ver. 3.2.2) codes were compared with the previous literature data and evaluated data of the JEFF-3.3, ENDF/B-VIII.0, JENDL/AD-2017 and TENDL-2019 libraries. A detailed analysis of uncertainties in the efficiencies of the HPGe detector and present measured cross sections was studied by the covariance analysis

method. In addition, the different author's formulae were used to systematically study the $(n, 2n)$ reaction cross section of rhodium and antimony isotopes and the formulae of Chatterjee, Bychkov, Luo and Lu and Fink reproduce the cross section very well except for the Habbani formula. The theoretical calculations of the $(n, 2n)$ reaction cross section for ground, isomeric state and isomeric cross section ratio were performed using the statistical nuclear reaction codes TALYS (ver. 1.9) and EMPIRE (ver. 3.2.2). The calculated cross section differs in magnitude only due to different nuclear inputs and different nuclear reaction models in the theoretical calculations. The emission of particles and photons in CN is the dominant reaction mechanism just above the two neutron emission thresholds energy. The CN cross section depends on the OPs, NLDs, and γ-SFs statistical nuclear ingratiates. In conclusion, the cross section from the EMPIRE calculations is differed only due to the difference between the generalized superfluid and Gilbert Cameron level density models. This generalized superfluid level density model considered the deformation effect and played an essential role in describing the $(n, 2n)$ reaction cross section. We considered nuclear ingratiates OPs, Level density, pre-equilibrium and γSFs for comparisons in the EMPIRE and TALYS calculations. It is shown that the two nucleon OPs of Koning and Delaroche give the same results. Similarly, for the γ-SFs, the phenomenological Brink-Axel model used in EMPIRE and Kopecky-Uhl generalized the Lorentzian model used in the TALYS code. It is safe to say that EMPIRE and the TALYS calculations differ only from using different theoretical models. The TALYS calculations at energies above the 14 MeV saturated more rapidly compared to the EMPIRE calculation. Furthermore, when the probability of nuclear reaction is high, the excitation functions generated by pre-equilibrium models in the calculations are heavily influenced by different level densities. As a result, level densities have a significant impact on reaction cross sections. For these nuclear reactions, exciton model predictions are generally precise. These new sets of estimated cross section data, we believe will aid in the understanding of neutron induced $(n, 2n)$ processes. It is observed that more experimental data are needed in the high energy region to investigate the contribution of different reaction channels and to test the reliability of the theoretical calculations. The outcomes of the experiment discussed here will be used for the evaluation of nuclear data libraries, the verification of nuclear reaction models, and other fundamental applications.

Bibliography

[1] A. J. Koning, J. Blomgren, R. Jacqmin, *et al.*, Nuclear data for sustainable nuclear energy, JRC Scientific and Technical Reports No. EUR 23977 EN – 2009.

[2] P. Reimer, V. Avrigeanu, S. V. Chuvaev *et al.*, Phys. Rev. C 71, 044617 (2005).

[3] Keiichi Shibata, Jour. of Nucl. Sci. and Tech., Vol. 51, No. 4, 425–436 (2014).

[4] V. P. Singh, *et al.*, Indian Journal of Pure & Applied Phys. Vol. 54, pp.443-448 (2016).

[5] N. Patronis C. T. Papadopoulos, *et al.*, Phys. Rev. C 75, 034607 (2007).

[6] E. Georgali, Z. Eleme, N. Patronis, *et al.*, Phys. Rev. C 98, 014622 (2018).

[7] N. Otuka, E. Dupont, V. Semkova *et al.*, Experimental Nuclear Reaction Data Library (EXFOR), Nuclear Data Sheets, Vol. 120, 272-276 (2014).

[8] R. Capote, *et al.*, IRDFF-II, Tech. Rep. INDC (NDS)-0616, IAEA-Vienna, (2012).

[9] Arjan Plompen, *et al.*, the JEFF-3.3 Nuclear Data Library, Nov. (2017).

[10] K. Shibata, N. Iwamoto, S. Kunieda, *et al.*, "JENDL/AD-2017" "Activation Cross-section File for Decommissioning of LWRs" JAEA-Conf 2016-004, pp.47-52.

[11] D. A. Brown, *et al.*, "EDNF/B-VIII.0." Nuclear Data Sheets 148, 1-142 (2018).

[12] A. J. Koning, *et al.*, "TENDL-2019" Nuclear data sheets Vol. 155, 1-55 (2019).

[13] Zhigang Ge, Ruirui Xu, *et al.*, "CENDL-3.2: The new version of Chinese general purpose evaluated nuclear data library" EPJ Web of Conferences 239, 09001 (2020).

[14] O. Iwamoto, K. Shibata, *et al.*, "Japanese Evaluated Nuclear Data Library version 5: JENDL-5.0", to be submitted (2022).

[15] R. A. Forrest, R. Capote, N. Otsuka, *et al.*, FENDL-3.2b Fusion Evaluation Nuclear Data Library, IAEA, INDC (NDS)-0628 (2022).

[16] A. J. Koning, *et al.*, TALYS (ver. 1.9), A Nuclear reaction program, user manual, NRG-1755 ZG Petten, The Netherlands (2018).

[17] M. Herman, R. Capote, *et al.*, " EMPIRE-3.2.3 Statistical Model Code for Nuclear Reaction Calculations and nuclear data evaluation" Nucl. Data Sheets 108, 2655 (2007).

[18] R. Capote, M. Herman, P. Oblozinsky *et al.*, "RIPL – Reference Input Parameter Library for Calculation of Nuclear Reactions and Nuclear Data Evaluations" Nuclear Data Sheets 110 (2009) 3107–3214.

[19] N. L. Das, C. V. S. Rao, B. V. T. Rao, J. R. Rao, Pramana, Vol.11, Issue.5, p.595 (1978).

[20] W. D. Lu, N. Ranakumar, *et al.,* Phys. Rev. Part C, Nucl. Phys. Vol. 1, p.350 (1970).

[21] S. K. Ghorai, J. E. Gaiser and W. L. Alford, J. Phys. G. Nucl. Phys. 6, 393-399 (1980).

[22] B. Minetti, A. Pasquarelli, Zeitschrift fuer Physik, Vol.217, p.83 (1968).

[23] R. Pepelnik, B. Anders, B. M. Bahal, M. Farooq, Report-GKSS- No. 86, E-29, (1986).

[24] M. Bormann, A. Behrend, *et al.*, Nuclear Physics, Section A Vol.115, 309 (1968).

[25] R. A. Jarjis, Nuclear Instruments and Methods, Vol. 184, Issues 2–3, 1, 439-444 (1981).

[26] J. Luo, Li Jiang, Long He, Applied Radiation and Isotopes, Vol. 140, 115-120, (2018).

[27] J. L. Casanova, Report from misc. OECD countries to NEANDC, No.140, p.9 (1974).

[28] J. H. Mccrary, I. L. Morgan, American Physical Society, Vol. 5, 246, (1960).

[29] J. Araminowicz, J. Dresler, Inst. Badan Jadr. (Nucl. Res.), Swierk+Warsaw, Repts, No.1464, p.14 (1973).

[30] Y. Kanda, Journal of the Physical Society of Japan, Vol.24, p.17 (1968).

[31] A. Reggoug, G. Paic, M. Berrada, Annual Report, No.5, p.14 (1982).

[32] E. B. Paul, R. L. Clarke, Canadian Journal of Physics, Vol.31, p.267 (1953).

[33] L. A. Rayburn, Physical Review, Vol. 130, p.731 (1963).

[34] C. Carles, Comptes Rendus, Vol. 257, p.659 (1963).

[35] C. S. Khurana, H. S. Hans, Nuclear Physics, Vol. 28, p.560 (1961).

[36] D. R. Koehler, W. L. Alford, Div. of Tech. Info. U.S. AEC Reports, No.11667 (1962).

[37] E. Rurarz, Z. Haratym, *et al.* Acta Physica Polonica, Part B, Vol.1, p.415 (1970).

[38] S. K. Mangal, P. S. Gill, Nuclear Physics, Vol. 49, p.510 (1963).

[39] N. Fotiades, M. Devlin, R. O. Nelson, *et al.*, Phys. Rev. C 94, 044608 (2016).

[40] A. A. Filatenkov, "Neutron Activation Cross Sections Measured at KRI in Neutron Energy Region 13.4 – 14.9 MeV" IAEA Nuclear Data Section, Vienna International Centre, A-1400 Vienna, Austria (2016).

[41] A. Paulsen and R. Widera, Z. Physik 238, 23-- 34 (1970).

[42] J. Laurec, A. Adam, 'Etudes Nucleaires, Saclay Reports, No.5109 (1981).

[43] W. D. Lu, *et al.,* Physical Review, Part C, Nuclear Physics, Vol. 1, p.350 (1970).

[44] M. Bormann, H. H.Bissem, *et al.,* Nuclear Physics, Section A, Vol. 157, p.481 (1970).

[45] J. Frehaut, A. Bertin, *et al.,* U.S. report to the I.N.D.C., No.84, Vol. (1), p.399 (1980).

[46] L. R. Veeser, E. D. Arthur, and P. G. Young, Phys. Rev. C Vol. 16, No. 5 (1977).

[47] D. S. Mather, P. F. Bampton, *et al.,* "Measurement of (n, $2n$) Cross Sections For Incident Energies Between 6 and 14 MeV" United Kingdom: N. P., (1972).

[48] D. G. Vallis," Cross sections for (n, $2n$) reaction at 14.7 MeV of some odd-proton nuclei." A.W.R.E. Aldermaston Reports, No.76/66 (1966).

[49] H. A.Tewes, A.A.Caretto, *et al.*, 'Excitation functions of neutron-induced reactions' U.C., Lawrence Rad.Lab. (Berkeley and Livermore), No.6028-T (1960).

[50] S. Chatterjee and A. Chatterjee, Nucl. Phys. A 125, 593 (1963).

[51] W. Lu, R.W. Fink, Phys. Rev. C 4 1173 (1971).

[52] J. Luo, F. Tuo, *et al.*, Nucl. Instrum. Methods Phys. Res. B 266 4862-4868 (2008).

[53] V. M. Bychkov, *et al.*, INDC (CCP)-146, IAEA-NDS, 1980. Vienna, Austria.

[54] F. I. Habbani and K. T. Osman, Appl. Radiat. Isot. 54 283-290 (2001).